and D. Wolf, "Actively mode-locked external-cavity semiconductor lasers with transform-limited single pulse output," *Opt. Lett.*, vol. 17, pp. 868–870, June 1992.
[5] D. J. Derickson, R. J. Helkey, A. Mar, and J. E. Bowers, "Suppression of multiple pulse formation in external cavity mode-locked lasers using intra-waveguide saturable absorbers," *IEEE Photon. Technol. Lett.*, vol. 4, pp. 333–335, Apr. 1992.
[6] D. Botez, L. J. Mawst, G. L. Peterson, and T. J. Roth, "Phase-locked arrays of antiguides: Modal content and discrimination," *J. Quantum Electron.*, vol. 26, pp. 482–495, Mar. 1990.
[7] A. Mar, J. D. Dudley, E. L. Hu, and J. E. Bowers, "Reactively sputtered silicon oxynitride for anti-reflection optical coatings," *Electronic Materials Conference*, Santa Barbara, CA, Oct. 1990.
[8] J. E. Bowers, P. A. Morton, S. Corzine, and A. Mar, "Actively mode locked semiconductor lasers," *J. Quantum Electron.*, vol. 25, pp. 1426–1439, June 1989.
[9] J. P. van der Ziel, H. Temkin, R. D. Dupuis, and R. M. Mikulyak, "Mode-locked picosecond pulse generation from high power phase-locked GaAs laser arrays," *Appl. Phys. Lett.*, vol. 44, Feb. 1984.
[10] H. Masuda and A. Takada, "Picosecond optical pulse generation from mode-locked phased laser diode array," *Electron. Lett.*, vol. 25, pp. 1418–1419, Oct. 1989.
[11] M. Segev, Y. Ophir, B. Fischer, and G. Eisenstein, "Mode locking and frequency tuning of a laser diode array in an extended cavity with a photorefractive phase conjugate mirror," *Appl. Phys. Lett.*, vol. 57, Dec. 1990.
[12] J. C. Kuo, C. S. Chang, and C. L. Pan, "Buildup of steady-state picosecond pulses in an actively mode-locked laser-diode array," *Opt. Lett.*, vol. 16, pp. 1328–1330, Sept. 1991.

High-Speed Vertical-Cavity Surface Emitting Laser

G. Shtengel, H. Temkin, *Fellow, IEEE,* P. Brusenbach, *Member, IEEE,* T. Uchida, M. Kim, C. Parsons, W. E. Quinn, and S. E. Swirhun, *Member, IEEE*

***Abstract*—We describe planar, gain-guided vertical-cavity surface emitting lasers with a modulation bandwidth of 14 GHz. This bandwidth is reached at a drive current of only 8 mA. The intrinsic bandwidth of these devices is estimated to be greater than 50 GHz. Nonlinear light-current characteristics of these lasers may lead to a high level of nonlinear harmonic distortion of the high-frequency output. We show that the relative intensity of the second harmonic response decreases rapidly at higher drive currents, in agreement with a phenomenological model based on the dc characteristics of the laser.**

THE POSSIBILITY of high-speed operation at low bias currents is one of the most attractive features of vertical-cavity surface emitting lasers (VCSEL's). This arises from the small active layer volume and high photon density. Considerable progress has been achieved recently in improving the continuous wave (CW) parameters of VCSEL's such as peak optical power, operating voltage, and thermal resistance [1], [2]. However, the modulation properties of VCSEL's remain restricted by parasitics resulting from the high p-type mirror resistance and, probably, transport effects [3], [4]. Although relaxation oscillations at frequencies as high as 70 GHz have been observed, confirming the high intrinsic bandwidth [5], the modulation bandwidths achieved thus far have been limited to approximately 8 GHz for gain-guided lasers [6] and about 5 GHz for index-guided lasers [7].

We report a significant improvement in the modulation bandwidth, of up to 14 GHz at a bias current of only 8 mA, of completely planar, gain-guided VCSEL's. We also study the modulation efficiency and the effects of nonlinear harmonic distortion arising in such lasers from the nonlinear light-current characteristics.

Two types of lasers, emitting at 0.96 and 0.78 μm, were used in this work. The epitaxial structures consisted of a bottom n-type Bragg reflector, a single-wavelength cavity, and a top p-type reflector. The bottom quarter-wavelength layers comprising the high-reflectivity mirrors consisted of AlAs/GaAs (23.5 periods) and AlAs/$Al_{0.3}Ga_{0.7}As$ (30.5 periods) for the 0.96- and 0.78-μm lasers, respectively. These mirrors were doped with Si to $n = 1.5 \cdot 10^{18}$ cm^{-3}. The p-type top mirrors (the output couplers) consisted of 16.5 and 23.5 periods, respectively, and were doped with C to $p = 3 \cdot 10^{18}$ cm^{-3}. The p-type mirrors had compositionally graded interfaces. The active region of the 0.96-μm laser contained three quantum-wells (QW's) of $In_{0.2}Ga_{0.8}As$, each being 8 nm thick and separated by 10-nm thick barriers of GaAs. The active layer of the 0.78-μm laser was a 52-nm thick layer of $Al_{0.15}Ga_{0.85}As$. Proton implantation was used for isolation and gain guiding. Both wafers received an initial implant that extended from the top surface through the active layers. The 780-nm wafer also received a second implant centered at the active layer and defining a slightly smaller aperture (by approximately 20%) than the first implant. The structures

Manuscript received July 29, 1993; revised October 4, 1993.
G. Shtengel and H. Temkin are with the Department of Electrical Engineering, Colorado State University, Ft. Collins, CO 80523.
P. Brusenbach, T. Uchida, M. Kim, C. Parsons, W. E. Quinn, and S. E. Swirhun are with Bandgap Technology Corporation, Broomfield, CO 80021.
IEEE Log Number 9214045.

were grown by molecular-beam epitaxy (MBE) on 3-in diameter wafers. The combination of structures and processes allows for comparisons between the bulk and QW lasers and to ascertain the importance of the carrier transport effects.

Fig. 1 presents the CW light-current characteristics of the 0.96-μm lasers of different sizes. Threshold currents were 4–7 mA and did not vary significantly with the laser diameter. This is expected in lasers with only the initial implant, in which the leakage currents are relatively larger in smaller-diameter devices. Threshold voltages were 3.1 V and 4.3 V for 15-μm lasers and 8-μm diameter lasers, respectively. At the operating current, the series resistance was in the range of 150–200 Ω. The maximum output powers were 2.2 mW for 15-μm diameter laser and 0.8 mW for 8-μm diameter. The 8-μm diameter lasers showed single-mode operation from threshold to the maximum power output. Larger devices showed higher-order transverse modes. The 0.78-μm lasers showed similar threshold currents of 4–6 mA, decreasing slightly with device size. A maximum power output of 0.3 mW and 0.4 mW was reached in 6- and 8-μm diameter lasers, respectively. Lower-output powers are expected in shorter-wavelength lasers. The threshold voltage of the 0.78-μm lasers was 3.4 V for 15-μm lasers and 3.2 V for 8-μm samples. All of these doubly implanted devices displayed a fundamental transverse mode behavior.

Small signal modulation measurements were carried out for all of the laser dimensions available. The optical response was collected by a fast PIN detector (20 GHz rolloff) and was analyzed by a spectrum analyzer under computer control. Fig. 2 shows two sets of the output power versus modulation frequency (at 0 dBm) characteristics, at different bias levels, for the 8-μm lasers. For the 0.96-μm laser, a maximum modulation bandwidth of 9.75 GHz was obtained at a bias of 10 mA, which corresponds to the optical power of 0.7 mW. The bandwidth decreases with increasing device size and reaches 6.5 GHz for the 15-μm devices. The bandwidth of 0.78-μm lasers, illustrated in Fig. 2(b), reached 14 GHz at a bias of only 8.0 mA.

The modulation data can be analyzed by using the procedure of Olshansky *et al.* [8]. This procedure is correct only for highly linear lasers, and it tends to overestimate the maximum bandwidth of lasers with sublinear light-current characteristics. The resonant frequencies of the 0.96-μm VCSEL plotted against the square root of optical power do not demonstrate a wide region of linearity, but have a rather high slope (the D coefficient) of 10 GHz/$\sqrt{\text{mW}}$, which is the highest reported thus far for VCSEL's. Fitting the modulation response curves allows us to extract the damping rates. A large Γ factor of about 10 GHz is obtained even at low optical powers, most likely as the result of lateral carrier diffusion across the active layer. This, together with low optical power, limits the modulation bandwidth. In this respect, there appears to be little difference between the bulk and QW-based lasers. Plotting the damping rate as a function of the resonance

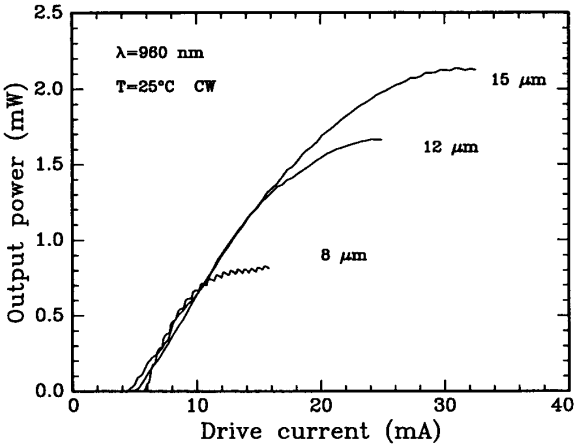

Fig. 1. Output power-drive current characteristics for 0.96-μm VCSEL's with three different diameters.

frequency square allows us to estimate the k factor as $k = 0.156$ nsec and the intrinsic bandwidth $f_{\max} > 50$ GHz. This is consistent with the relaxation-oscillation measurements of Tauber *et al.* [5]. Surprisingly, the faster 0.78-μm lasers show a higher damping rate of more than 20 GHz and a lower intrinsic bandwidth. Clearly, both types of lasers studied here suffer from high parasitics, especially p-type mirror resistance, and their frequency dependence is not yet understood.

The high bandwidth measured in our VCSEL's can be attributed to a number of factors. The resistance of the top mirror was reduced to $\sim 95\ \Omega$ as a result of C-doping. The p-side metallization, formed by small ($50 \times 50\ \mu\text{m}^2$) contact pads, was carefully annealed. This minimizes the resistance and capacitance of the p-metal. Finally, the measurements were carried out using high-speed ground-signal-ground probes. The ground plane was brought up to the probe level by an Au-plated via hole in a coplanar waveguide fixture bonded next to the laser.

High nonlinearities observed in light-current characteristics of these lasers lead to a high level of nonlinear harmonic distortion of the high frequency output. We used the phenomenological model of Takemoto *et al.* [9] to estimate the intensity of the second harmonic from the CW light-current curves. Writing the optical power output P as follows:

$$P = A + B \cdot I + C \cdot I^2 \tag{1}$$

where I is drive current and A, B, and C are the fitting coefficients, gives the correlation between the fundamental and second harmonic, provided that the drive current can be written as $I(t) = I_0 + I_1 \cdot \sin(\omega t)$. The relationship between the fundamental and the second harmonic may be then written as follows:

$$\frac{P_1^2}{P_2} = 2 \cdot \left| \frac{(B + 2 \cdot C \cdot I_0)^2}{C} \right| \tag{2}$$

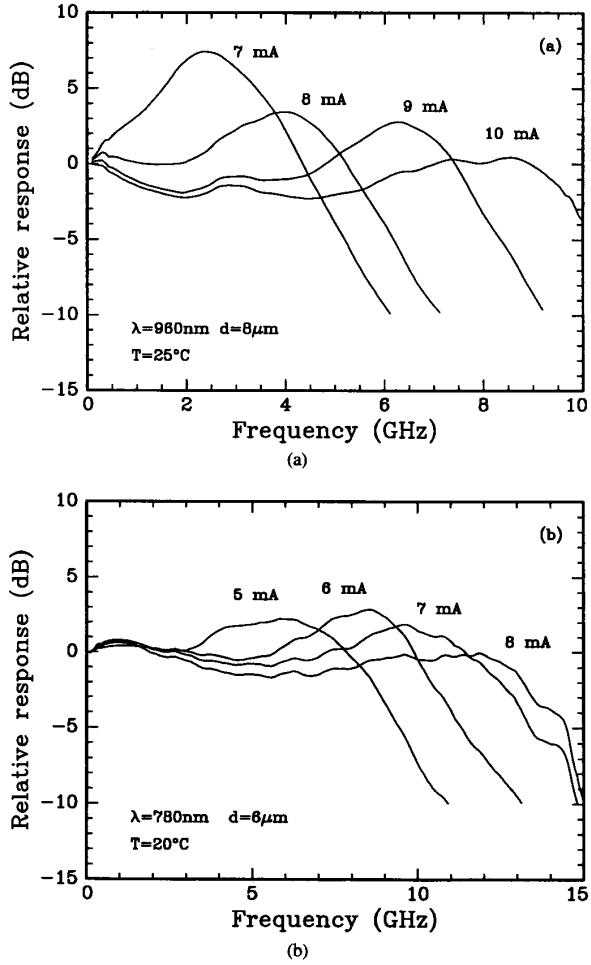

Fig. 2. Two sets of modulation frequency characteristics at different bias levels. (a) The 0.96-μm laser fabricated by a single proton isolation. (b) The 0.78-μm laser fabricated with an additional second implant centered at the active layer. Modulation bandwidths of 10 and 14 GHz, respectively, are obtained.

where $P(t) = P_0 + P_1 \cdot \sin(\omega t) + P_2 \cdot \sin(2\omega t)$.

Fig. 3 shows the measured fundamental and second harmonic response of a 0.96-μm laser at a bias $I_0 = 1.1I_{th}$. We also show a fit obtained for the second harmonic, calculated by using the fundamental harmonic response and (2). Several response curves recorded at different modulation depths (i.e., at different I_1) are used to normalize the dependence. Excellent agreement between the measured high frequency response and the calculation derived from the CW data is evident, even though at the small drive currents of VCSEL's, the measured dynamic response may not be the true small-signal response. Similar results are obtained for the 0.78-μm lasers.

The inset of Fig. 3 summarizes the experimental and calculated suppression of the second harmonic dependence on the drive current, normalized to the threshold current. While the second harmonic is only 5 dB below

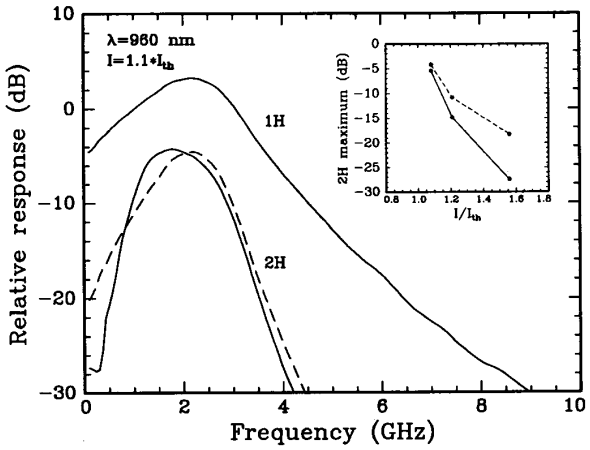

Fig. 3. Experimental curves (solid) for the fundamental and second harmonic modulation response. The second harmonic response (dashed) was calculated by using a model based on the nonlinearity of the light-current characteristics. The inset shows experimental (solid) and calculated (dashed) second harmonic response dependence on the drive current.

that of the fundamental harmonic at low currents, the relative intensity of the second harmonic response decreases rapidly at higher currents. Our model does not take into account electron–photon resonance in the cavity, so it cannot satisfactorily explain the laser behavior at high powers, where the second resonant peak appears at half the resonant frequency. The correct solution can be obtained from rate equations [10], [11].

In conclusion, we have prepared VCSEL's with the highest modulation bandwidth of 14 GHz at a drive current of only 8 mA. This is the fastest VCSEL described thus far. We also measure the highest value of the coefficient $D = 10$ GHz/$\sqrt{\text{mW}}$ yet reported. We show that nonlinear harmonic distortion can be accurately described by a simple model based on CW light-current characteristics. The second harmonic intensity decreases rapidly at higher drive currents.

REFERENCES

[1] M. G. Peters, F. H. Peters, D. B. Young, J. W. Scott, B. J. Thibeault, and L. A. Coldren, "High wallplug efficiency vertical-cavity surface-emitting lasers using lower barrier DBR mirrors," *Electron. Lett.*, vol. 29, pp. 170–172, 1993.

[2] D. Vakshoori, J. D. Wynn, and G. J. Zydzik, R. E. Leibenguth, M. T. Asom, K. Kojima, and R. A. Morgan, "Top-surface emitting lasers with 1.9 V threshold voltage and the effect of spatial hole burning on their transverse mode operation and efficiencies," *Appl. Phys. Lett.*, vol. 62, pp. 1448–1450, 1993.

[3] M. G. Peters, M. L. Majewski, and L. A. Coldren, "Intensity modulation bandwidth limitations of vertical-cavity surface-emitting laser diodes," *Quantum Optoelectron. Topical Meeting*, pp. 60–61, Palm Springs, CA, 1993.

[4] M. Ishikawa, R. Nagarajan, T. Fokushima, J. G. Wasserbauer, and J. E. Bowers, "Long wavelength high-speed semiconductor lasers with carrier-transport effects," *IEEE J. Quantum Electron.*, vol. 28, pp. 2230–2241, 1992.

[5] D. Tauber, G. Wang, R. S. Geels, J. E. Bowers, and L. A. Coldren, "Large and small signal dynamics of vertical cavity surface emitting lasers," *Appl. Phys. Lett.*, vol. 62, pp. 325–327, 1993.

[6] F. S. Choa, Y. H. Lee, T. L. Koch, C. A. Burrus, B. Tell, J. L.

Jewell, and R. E. Leibenguth, "High-speed modulation of vertical-cavity surface emitting lasers," *IEEE Photon. Technol. Lett.*, vol. 3, pp. 697–699, 1991.
[7] G. Hasnain, K. Tai, N. K. Dutta, Y. H. Wang, J. D. Wynn, B. E. Weir, and A. Y. Cho, "High temperature and high frequency performance of gain guided surface emitting lasers," *Electron. Lett.*, vol. 27, pp. 915–916, 1991.
[8] R. Olshansky, P. Hill, V. Lanzisera, and W. Powazinik, "Frequency response of 1.3 μm InGaAsP high speed semiconductor lasers," *IEEE J. Quantum Electron.*, vol. QE-23, pp. 1410–1418, 1987.
[9] A. Takemoto, H. Watanabe, Y. Nakajima, Y. Sakakibara, S. Kakimoto, J. Yamashita, T. Hatta, and Y. Miyake, "Distributed feedback laser diode and module for CATV systems," *IEEE J. Select. Areas in Commun.*, vol. 8, pp. 1359–1364, 1990.
[10] A. Oliver, Ph.D. dissertation, Academie de Lille, Flanders, Artois, pp. 65–91, 1991.
[11] T. E. Darcie, R. S. Tucker, and G. J. Sullivan, "Intermodulation and harmonic distortion in InGaAsP lasers," *Electron. Lett.*, vol. 21, pp. 665–666, 1985.

Transform-Limited Optical Short-Pulse Generation at High Repetition Rate over 40 GHz from a Monolithic Passive Mode-Locked DBR Laser Diode

Shin Arahira, Yasuhiro Matsui, Tatsuo Kunii, Saeko Oshiba, and Yoh Ogawa

Abstract—**We fabricated a monolithic passive mode-locked distributed Bragg reflector laser diode for the first time. An optical short-pulse train with a duration of 3.5 ps was successfully generated from the laser at a high repetition rate of over 40 GHz. The time-bandwidth product was 0.43, and it was very close to the transform-limited value of a Gaussian waveform. The highest peak power of 60 mW in an InP-based passive mode-locked laser has been achieved. This laser is promising as an optical source for a high bit rate soliton transmission system.**

INTRODUCTION

THEORETICAL and experimental research on optical soliton transmission have proved its advantages, such as longer transmission distance limitation compared to that of conventional intensity modulation/direct detection (IM/DD) systems [1]–[6]. It has been pointed out that optical soliton transmission is promising for the realization of high bit rate optical transmission systems over 10 Gb/s. In high bit rate optical soliton transmission systems, the development of an optical pulse source that generates picosecond, transform-limited pulses is required. It is hard to obtain such optical pulses by a gain-switched distributed feedback (DFB) laser diode, which has been used for the optical source of soliton transmission [7], because the available repetition rate of a gain-switched DFB laser is restricted by its electrical bandwidth, which is 20 GHz at most. Also, the pulse generated from a gain-switched DFB laser has nonlinear chirp. A mode-locking technique is an alternate method by which obtain ultrashort optical pulse train with transform-limited condition. A mode-locked semiconductor laser diode (LD) can generate an ultrashort optical pulse train of picosecond or subpicosecond duration at a high repetition rate, because of a wide ($\sim$ 25 nm) gain bandwidth and a short cavity length. There have been several reports on passive [8]–[11] and active [12]–[14] mode-locked LD's with external cavities or monolithic structures. However, an external cavity LD suffers in its performance from the mechanical instabilities and poor intracavity coupling efficiency. In addition, the repetition rate of the mode-locked external cavity LD is relatively low because of its long cavity length. Therefore, a monolithic mode-locked LD is desired to make the best use of the advantages of the LD. In this letter, we report on passive mode-locking at a repetition rate of over 40 GHz using a monolithic four-electrode distributed Bragg reflector (DBR) LD.

Manuscript received June 29, 1993; revised August 16, 1993.
S. Arahira is with the Semiconductor Technology Laboratory, OKI Electric Industry Co., Ltd., Tokyo 193, Japan.
IEEE Log Number 9213974.

DEVICE STRUCTURE

The DBR-LD used in this study was fabricated by using MO-VPE crystal growth. The schematic cross-section of the LD is shown in Fig. 1. The LD has four electrodes corresponding to a saturable absorber, a gain, a phase control, and a DBR section, respectively. The sections are separated by 20-μm wide stripe and have 1-kΩ electrical isolation. The active layers of the gain and the absorber sections are composed of strained multiple quantum-well